Journal of Biomolecular NMR, **24:** 51–62, 2002.
KLUWER/ESCOM

Cα chemical shift tensors in helical peptides by dipolar-modulated chemical shift recoupling NMR

Xiaolan Yao, Satoru Yamaguchi* & Mei Hong**
Department of Chemistry, Iowa State University, Ames, IA 50011, USA

Received 22 May 2002; Accepted 2 August 2002

Key words: chemical shift tensor, dipolar modulation, helical peptides, icosahedral representation, solid-state NMR

Abstract

The Cα chemical shift tensors of proteins contain information on the backbone conformation. We have determined the magnitude and orientation of the Cα chemical shift tensors of two peptides with α-helical torsion angles: the Ala residue in G*AL ($\phi = -65.7°$, $\psi = -40°$), and the Val residue in GG*V ($\phi = -81.5°$, $\psi = -50.7°$). The magnitude of the tensors was determined from quasi-static powder patterns recoupled under magic-angle spinning, while the orientation of the tensors was extracted from Cα–Hα and Cα–N dipolar modulated powder patterns. The helical Ala Cα chemical shift tensor has a span of 36 ppm and an asymmetry parameter of 0.89. Its σ_{11} axis is $116° \pm 5°$ from the Cα–Hα bond while the σ_{22} axis is $40° \pm 5°$ from the Cα–N bond. The Val tensor has an anisotropic span of 25 ppm and an asymmetry parameter of 0.33, both much smaller than the values for β-sheet Val found recently (Yao and Hong, 2002). The Val σ_{33} axis is tilted by $115° \pm 5°$ from the Cα–Hα bond and $98° \pm 5°$ from the Cα–N bond. These represent the first completely experimentally determined Cα chemical shift tensors of helical peptides. Using an icosahedral representation, we compared the experimental chemical shift tensors with quantum chemical calculations and found overall good agreement. These solid-state chemical shift tensors confirm the observation from cross-correlated relaxation experiments that the projection of the Cα chemical shift tensor onto the Cα–Hα bond is much smaller in α-helices than in β-sheets.

Introduction

The chemical shift tensor of backbone Cα is an important probe of the conformation of peptides and proteins. It has long been recognized that Cα isotropic chemical shifts in α-helical and β-sheet conformations differ by an average of about 3.6 ppm (Spera and Bax, 1991; Wishart et al., 1991). But in addition to this isotropic shift difference, chemical shift anisotropy (CSA) is also sensitive to protein secondary structure (Sitkoff and Case, 1998). This was first observed in solution NMR xperiments that utilized relaxation interference between Cα–Hα dipolar coupling and Cα CSA to determine $\Delta\sigma^* = \Delta\sigma_{\rm orth} - \Delta\sigma_{\rm par}$, where $\Delta\sigma_{\rm par}$ is the shielding along the Cα–Hα bond and $\Delta\sigma_{\rm orth}$ is the average shielding orthogonal to it. These experiments found $\Delta\sigma^*$ to be 6.1 ± 4.9 ppm in helical residues but 27.1 ± 4.3 ppm in sheet residues (Tjandra and Bax, 1997). Quantum chemical calculations revealed that for β-branched amino acids such as Val and Ile, the span of the Cα shielding tensor, $\Omega = \sigma_{33} - \sigma_{11}$, is larger in sheet than in helix, but the non-β-branched amino acids do not show such a clear magnitude difference (Havlin et al., 1997). Calculations also indicated that the orientation of the Cα shielding tensor changes significantly between helix and sheet, causing the projection of the shielding tensor onto the Cα–Hα bond to be especially different (Walling et al., 1997). Direct solid-state NMR measurements in ubiquitin confirmed the differences in the tensor span Ω between helix and sheet for resolved residues (Hong, 2000). These measured span differences are much smaller than the $\Delta\sigma^*$ difference observed in solution. This was re-

*Current address: Department of Life Science, Himeji Institute of Technology, Harima Science Garden City, Kamigori, Hyogo 678-1297, Japan.
**To whom correspondence should be addressed. Fax: +1-515-294-0105, E-mail: mhong@iastate.edu

cently found to be a result of the difference in the Cα shielding tensor orientations. When experimentally measured chemical shift spans Ω of several solid peptides were converted to $\Delta\sigma^*$ using the calculated tensor orientations, good agreement was found with the $\Delta\sigma^*$ values of globular proteins in solution (Havlin et al., 2001).

Therefore, the orientation of the Cα shielding tensor is an important conformation-dependent parameter and may be more generally sensitive to peptide backbone torsion angles than the magnitude of the tensor. Until recently, this orientation information was not easily accessible from solid-state NMR, due to the difficulty of specifically labeling ^{13}Cα and ^{15}N in most amino acids except for Gly. ^{15}N labeling is necessary for accurate determination of the Cα tensor, since it enables both decoupling of the ^{15}N-^{13}Cα dipolar interaction and the use of ^{15}N-^{13}Cα dipolar coupling to compare with the orientation of the Cα shielding tensor. Uniform ^{13}C labeling is undesirable, since the homonuclear ^{13}C-^{13}C couplings significantly complicate the determination of the ^{13}Cα chemical shift tensor. The lack of ^{13}Cα and ^{15}N double labeling prevented the use of static dipolar modulation experiments on powder samples to measure the chemical shift tensor orientation and magnitude (Hartzell et al., 1987; Hartzell et al., 1987). Meanwhile, single crystals of model peptides are generally difficult to obtain, thus precluding the use of rotation patterns for Cα tensor determination. These limitations prompted us recently to develop a general solid-state NMR technique to determine the Cα tensor orientations on powder samples without ^{13}C labeling but with ^{15}N labeling (Yao and Hong, 2002). Our approach utilizes the recently developed 2D SUPER experiment (Liu et al., 2002) to first recouple the CSA interaction under magic-angle spinning (MAS). This yields quasi-static powder patterns in the indirect dimension of a 2D spectrum. The tensor orientation is then measured by modulating these CSA powder patterns with ^{13}Cα–^{1}Hα and ^{13}Cα–^{15}N dipolar couplings (Yao and Hong, 2002). As a result, the orientation of the Cα shielding tensor relative to the Cα-Hα bond and the Cα-N bond is determined.

We previously applied this dipolar-modulated CSA recoupling technique to N-acetyl-valine (NAV), a model amino acid with β-sheet torsion angles (Carroll et al., 1990). NAV Cα has a relatively large CSA span of 46.5 ppm, and the σ_{11} axis is close to parallel (22°) to the Cα–Hα bond (Yao and Hong, 2002). In this work, we determine the complete Cα chemical shift tensors of alanine and valine in two helical peptides to compare with the β-sheet case. The two helical peptides, GG*V-OH and G*AL-OH, where Val and Ala were ^{15}N labeled, were chosen due to their known crystal structures (Chaturvedi et al., 1991; Lalitha et al., 1984). The Val residue in GG*V has torsion angles of $\phi = -81.5°$ and $\psi = -50.7°$, while the Ala residue in G*AL has torsion angles of $\phi = -65.7°$ and $\psi = -40°$. Both residues were ^{15}N labeled to allow ^{13}C–^{15}N dipolar modulation of the Cα powder patterns and to permit complete decoupling of nitrogen during the ^{13}C chemical shift evolution. We found that the Cα tensor of these helical residues has very different orientations and magnitudes from that of the β-sheet Val.

Materials and methods

Peptide synthesis and purification

Wang resin, Fmoc-Leu-Wang resin and Fmoc-Gly were purchased from Novabiochem (San Diego, CA).^{15}N-Fmoc-alanine and ^{15}N-Fmoc-valine were purchased from Cambridge Isotope Laboratories (Andover, MA). The ^{15}N-labeled G*AL–OH and GG*V–OH were synthesized by Fmoc solid-phase peptide synthesis methods and cleaved with trifluoroacetic acid. ^{15}N-Fmoc-valine was linked to Wang resin using a symmetrical anhydride (Synthesis notes, Novabiochem). The identities of the peptides were confirmed by electron spray ionization mass spectrometry, ^{1}H solution NMR and ^{13}C solid-state NMR. The crude peptides were purified by ion exchange chromatography and recrystallized by slow evaporation from water at 4 °C. The crystal structure of the synthesized GAL was directly determined by X-ray crystallography and found to be identical to that shown in the literature (Chaturvedi et al., 1991). The crystal structure of GGV was not directly measured due to the small sizes of the crystallites. However, the labeled GGV exhibited identical ^{13}C and ^{1}H isotropic chemical shifts with those of the commercially available, unlabeled, GGV. Further, repeated recrystallization of GGV always yielded the same NMR spectra, indicating that the molecular conformation of this peptide is extremely stable and that the molecule is unlikely to have a second conformation.

NMR experiments

All NMR experiments were carried out on a Bruker DSX-400 spectrometer (Karlsruhe, Germany) at a magnetic field of 9.4 Tesla. A triple-resonance MAS probe with a 4-mm spinning module was used for the experiments. Standard 90° pulse lengths were 3.5 μs for ^{1}H and 5 μs for ^{13}C and ^{15}N. The ^{1}H decoupling field strength was 75 kHz during acquisition and 85–95 kHz during the evolution period. A ^{15}N decoupling field of about 20 kHz was used during ^{13}C evolution. Cross polarization (CP) spin-lock fields of 50 kHz were used, and the contact time was typically 500 μs except in the C-H dipolar modulation experiments. The indirect dimension of the 2D experiments was incremented synchronously with sample rotation, which was typically at a speed of 2.5 kHz. Due to the scaling factor of 0.155 for the CSA recoupling sequence, the effective t_1 dwell time was $\tau_r \times 0.155 = 400\ \mu s \times 0.155 = 62\ \mu s$. This effective dwell time was used in data processing. Recycle delays were 1.5–3 s. Signal-averaging time for the 2D experiments ranged from 8 h to 22 h. Typical line broadening was 60 Hz in the direct dimension and 40–100 Hz in the indirect dimension. All ^{13}C chemical shifts were referenced to the carbonyl line of external glycine at 176.4 ppm relative to TMS.

We describe the CSA magnitudes by the anisotropic span Ω, defined as $(\delta_{11} - \delta_{3}3)/(1 - \sigma_{ref}) \approx \delta_{11} - \delta_{33}$, where the three principal values follow the convention $\delta_{11} \geq \delta_{22} \geq \delta_{33}$ (Jameson, 1998). The symmetry of the CSA tensor is described by the asymmetry parameter, η, which is defined as $(\delta_{22} - \delta_{11})/(\delta_{33} - \delta_{iso})$ when δ_{11} is closer to the isotropic shift, and $(\delta_{22} - \delta_{33})/(\delta_{11} - \delta_{iso})$ when δ_{33} is closer to the isotropic shift (Duncan, 1997; Schmidt-Rohr and Spiess, 1994). We report the experimentally measured principal values on the δ scale, but the principal axis orientations by the shielding notation σ.

Pulse sequences

The unmodulated CSA powder spectra were measured using the SUPER sequence shown in Figure 1(a) (Liu et al., 2002). During the t_1 period, the ^{13}C CSA interaction is recoupled by 2π pulses placed at specific time points in each rotor period calculated to yield undistorted powder patterns. This recoupling sequence is an improvement over the original Tycko experiment (Tycko et al., 1989) by replacing π pulses with better compensated 2π pulses. The quasi-static powder patterns, which are independent of the MAS spinning

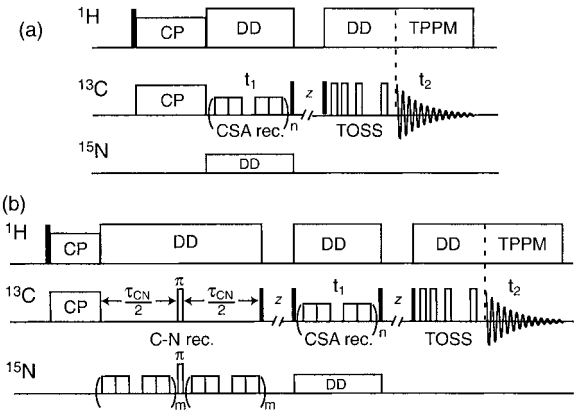

Figure 1. Pulse sequences for determining the orientation of the Cα chemical shift tensor. (a) SUPER experiment. With a short ^{1}H-^{13}C CP contact time, this is also the Cα–Hα modulation experiment. (b) Cα–N modulation experiment. DD: dipolar decoupling. TOSS: total sideband suppression (Dixon, 1982). TPPM: two-pulse phase modulation (Bennett et al., 1995).

speeds, yield accurate principle values. C–H dipolar modulation of the powder patterns is achieved by using a short CP contact time of about 20 μs (Yao and Hong, 2002). During this short time, the Cα–Hα dipolar coupling is minimally affected by the slow sample rotation, and thus modulates the CSA spectra according to the relative orientation of the chemical shift tensor to the Cα–Hα bond. Cα–N modulation of the CSA spectra is achieved by recoupling the ^{13}Cα-^{15}N dipolar interaction for a fixed duration before the CSA evolution (Figure 1(b)). The ^{13}C-^{15}N dipolar interaction is recoupled by applying the same rotor-synchronized 2π pulses on the ^{15}N channel, since the SUPER sequence recouples all interactions linear in the spin of interest. Subsequently, the Cα–N dipolar-dephased ^{13}Cα magnetization evolves under the pure CSA interaction to yield a modulated powder pattern.

To confirm the result of the Cα–Hα modulation experiment on GGV, we carried out an additional experiment that *dephases* the Cα CSA spectrum according to the Cα–Hα dipolar coupling. This dephasing experiment is the opposite of the CP-based Cα–Hα build-up experiment, in that the principal value most closely parallel to the Cα–Hα bond has the lowest intensity rather than the highest intensity. The experiment differs from the original SUPER sequence only in the addition of a rotor-synchronized echo period of $2\tau_r$ after the CP step and before the t_1 evolution. At the beginning of this echo period, ^{1}H decoupling is turned off for a time short compared to the rotor period. In this way, Cα magnetization is dephased according to

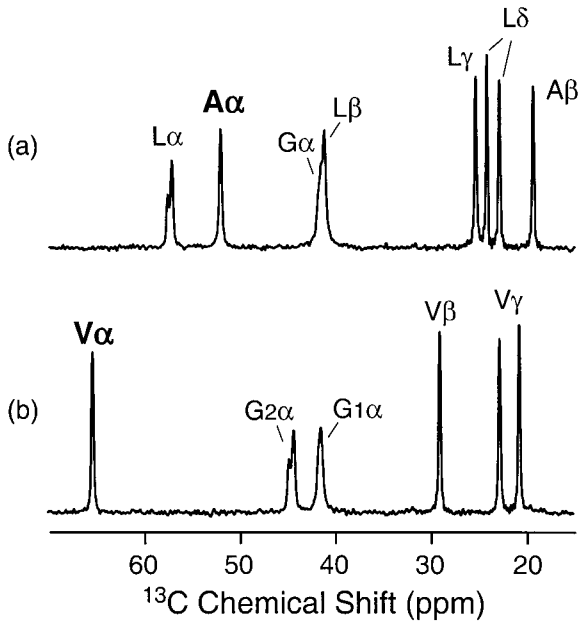

Figure 2. ^{13}C spectra of (a) GAL and (b) GGV. Spinning speed: 7 kHz.

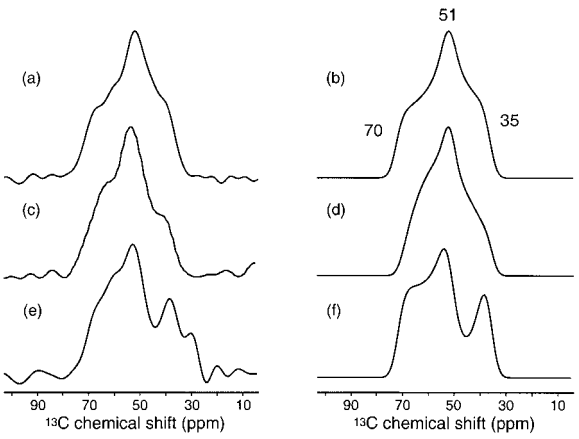

Figure 3. Recoupled CSA spectra of Ala Cα in G*AL. (a) SUPER spectrum without dipolar modulation. NS per t_1 slice = 192. (b) Best fit for (a), yielding the three principal values. (c) Cα–Hα modulated CSA spectrum, acquired with a CP contact time of 20 μs. NS per t_1 slice = 192. (d) Best fit for (c), using $\beta_{CH}(\sigma_{33}) = 70°$ and $\alpha_{CH}(\sigma_{33}) = 58°$. (e) Cα–N modulated CSA spectrum, acquired with a Cα–N dephasing time of 3.2 ms. NS per t_1 slice = 512. (f) Best fit for (e), using $\beta_{CN}(\sigma_{33}) = 56°$ and $\alpha_{CN}(\sigma_{33}) = 68°$. All 2D spectra were obtained with 44 t_1 slices and a maximum evolution time of 8.8 ms.

the relative orientation of the Cα–Hα bond to the Cα CSA tensor.

The radio-frequency field strength of the 2π pulses for CSA recoupling was 12.12 times the spinning speed. To minimize undesirable CP from ^{13}C to ^{1}H during CSA recoupling, a relatively slow spinning speed of 1.8 kHz to 2.5 kHz was used in the experiments. A TOSS sequence (Dixon, 1982) was applied before detection to remove the spinning sidebands.

Results and discussion

Ala spectra of GAL

Figure 2 shows the aliphatic region of the 1D ^{13}C MAS spectra of recrystallized GAL (a) and GGV (b). The isotropic shifts of Val and Ala Cα are 65.3 ± 0.3 ppm and 52.0 ± 0.3ppm, respectively. Compared to their respective random coil shifts of 61.4 ppm and 51.7 ppm (Wishart et al., 1991), these secondary shifts confirm the helical conformation of the Val and Ala residues. The line widths of the Cα peaks are 27 Hz (0.27 ppm) for Val and 31 Hz (0.31 ppm) for Ala, indicating that the peptides have homogeneous structures. For the residues that are not ^{15}N labeled, the second-order quadrupolar effects of ^{14}N, which cannot be completely averaged by MAS, are transferred to the directly bonded ^{13}C through dipolar coupling and cause splittings in the Leu Cα peak of GAL and the Gly2 Cα line of GGV (Figure 2) (Harris and Oliveri, 1992). However, the fast NH_3^+ rotational motions of the N-terminal glycine residues in both peptides remove this effect so that no splitting is observed for these Gly Cα peaks.

The Cα CSA spectra of Ala with and without dipolar modulation are shown in Figure 3. The unmodulated CSA spectrum is best fit with principal values of $\delta_{11} = 70$ ppm, $\delta_{22} = 51$ ppm, and $\delta_{33} = 35$ ppm (Figure 3(b)). Cα–Hα(N) dipolar modulation changed the powder pattern in a way that is indicative of the relative orientation between the Cα chemical shift tensor and the Cα–Hα(N) bond, respectively (Figure 3(c, e)).

To extract the chemical shift tensor orientation, we compared the experimental spectra with the calculated spectra as a function of the polar angle β and azimuthal angle α of the Cα–Hα(N) bond relative to the principal axis system (PAS) of the CSA tensor. The β and α angles are defined as shown in Figure 4: in a right-handed Cartesian coordinate system representing the chemical shift PAS, $\beta_{CH(N)}(\sigma_{33})$ is the polar or directional angle between the σ_{33} axis and the Cα–Hα(N) bond, while $\alpha_{CH(N)}(\sigma_{33})$ is the angle between the projection of the Cα–Hα(N) bond onto the σ_{11}-σ_{22} plane

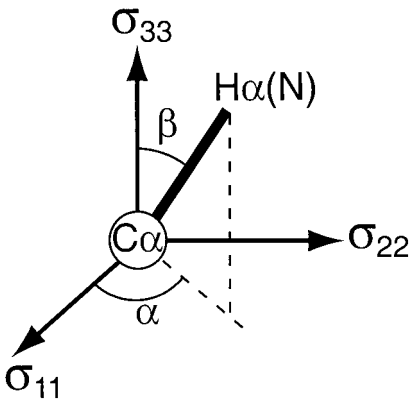

Figure 4. Definition of the polar coordinates α and β. Here the β angle corresponds to $\beta_{CH(N)}(\sigma_{33})$ while the α angle is $\alpha_{CH(N)}(\sigma_{33})$.

and the σ_{11} axis. With this definition, once the polar and azimuthal angles between the σ_{33} axis and the Cα–Hα(N) bond are determined, the other two directional angles, $\beta_{CH(N)}(\sigma_{11})$ and $\beta_{CH(N)}(\sigma_{22})$, can be readily calculated according to:

$$\cos[\beta_{CH(N)}(\sigma_{11})] = \cos[\alpha_{CH(N)}(\sigma_{33}] \sin[\beta_{CH(N)}(\sigma_{33})], \quad (1)$$

$$\cos[\beta_{CH(N)}(\sigma_{22})] = \cos[90^\circ - \alpha_{CH(N)}(\sigma_{33}] \sin[\beta_{CH(N)}(\sigma_{33})]. \quad (2)$$

Note that the orientation of the chemical shift tensor in the molecular frame is independent of the choice of the angles being used in the simulations. We could have simulated for $\beta_{CH(N)}(\sigma_{ii})$ and $\alpha_{CH(N)}(\sigma_{ii})$ (i = 1, 2) and would have obtained the same tensor orientation.

The experimental Cα–Hα modulated Ala Cα spectrum (Figure 3(c)) is best fit with $\beta_{CH}(\sigma_{33}) = 70^\circ$ and $\alpha_{CH}(\sigma_{33}) = 58^\circ$ (Figure 3(d)), while the Cα–N modulated powder pattern is best fit with $\beta_{CN}(\sigma_{33}) = 56^\circ$ and $\alpha_{CN}(\sigma_{33}) = 68^\circ$ (Figure 3(f)). To indicate the angular resolution of the dipolar modulation, we show several calculated Cα–Hα and Cα–N modulated CSA spectra with $\beta_{CH(N)}(\sigma_{33})$ and $\alpha_{CH(N)}(\sigma_{33})$ from 0° to 90° (Figure 5(a–b)). It can be seen that the modulated Cα CSA spectra of Ala are quite sensitive to both $\beta_{CH(N)}(\sigma_{33})$ and $\alpha_{CH(N)}(\sigma_{33})$ angles. When $\beta_{CH(N)}(\sigma_{33}) = 0^\circ$, the Cα–Hα(N) bond is along the σ_{33} direction, thus spectra with different α angles are identical. The best-fit angles for the experimental spectra were obtained from the minimum root-mean-square deviation (RMSD) between the experiment and the simulation. Figure 5(c) and (d) display the RMSD plots for the Cα–Hα and Cα–N modulated spectra, respectively, where the minimum RMSD value was normalized to 1. The contour plots show that both dipolar modulated experiments are more sensitive to variations in $\beta_{CH(N)}(\sigma_{33})$ than to changes in $\alpha_{CH(N)}(\sigma_{33})$. Since each orientation angle has a two-fold degeneracy in a 180° range, we only show the RMSD between 0° and 90° for both polar coordinates. The best fit for the Cα–Hα modulated Ala spectrum is $\beta_{CH}(\sigma_{33}) = 70^\circ \pm 5^\circ$ and $\alpha_{CH}(\sigma_{33}) = 58^\circ \pm 10^\circ$, while the best fit for the Cα-N modulated spectrum is $\beta_{CN}(\sigma_{33}) = 56^\circ \pm 5^\circ$ and $\alpha_{CN}(\sigma_{33}) = 68^\circ \pm 10^\circ$.

Val spectra of GGV

The Cα CSA spectra of Val in GGV with and without dipolar modulation are shown in Figure 6. The unmodulated CSA spectrum is best fit with principal values of $\delta_{11} = 75$ ppm, $\delta_{22} = 70$ ppm and $\delta_{33} = 51$ ppm (Figure 6(b)). The Cα–Hα modulated Val Cα spectrum (Figure 6(c)) is best fit with $\beta_{CH}(\sigma_{33}) = 65^\circ$ and $\alpha_{CH}(\sigma_{33}) = 20^\circ$ (Figure 6(d)), while the Cα–N modulated spectrum (Figure 6(e)) corresponds to $\beta_{CN}(\sigma_{33}) = 82^\circ$ and $\alpha_{CN}(\sigma_{33}) = 62^\circ$ (Figure 6(f)). These best fit angles were again obtained by comparing with the simulated spectra. As shown in Figure 7(a–b), the angular resolution for the Cα–Hα(N) modulation experiments is higher in the β angle than in the α angle.

In addition to the normal 180° degeneracy in the orientation determination, another near-degeneracy was observed in the GGV spectra. Figures 7(a) and (b) show that the spectral intensities at δ_{11} and δ_{22} frequencies are similar regardless of the orientation angles. This arises from the near uniaxiality of the Val CSA tensor ($\eta = 0.33$), where the δ_{11} and δ_{22} principal values differ by only 5 ppm. For an exactly uniaxial CSA tensor, the σ_{11} and σ_{22} axes are equivalent, thus the orientation of the σ_{11} axis with the Cα–Hα(N) bond would be indistinguishable from the orientation of the σ_{22} axis. In contrast, the unique σ_{33} axis has an unambiguous orientation. This justifies our choice of simulating the experimental Val spectra using σ_{33} as the primary reference axis. One consequence of this near degeneracy is that the orientations of the σ_{11} and σ_{22} axes may be interchanged if care is not taken in analyzing the spectra. According to Equations (1) and (2), and using $\beta_{CH}(\sigma_{33}) = 65^\circ$ and $\alpha_{CH}(\sigma_{33}) = 20^\circ$, one obtains $\beta_{CH}(\sigma_{11}) = 32^\circ$ and $\beta_{CH}(\sigma_{22}) = 72^\circ$. However, the near degeneracy between the σ_{11} and σ_{22} axes could also mean that $\beta_{CH}(\sigma_{11}) = 72^\circ$ and $\beta_{CH}(\sigma_{22}) = 32^\circ$.

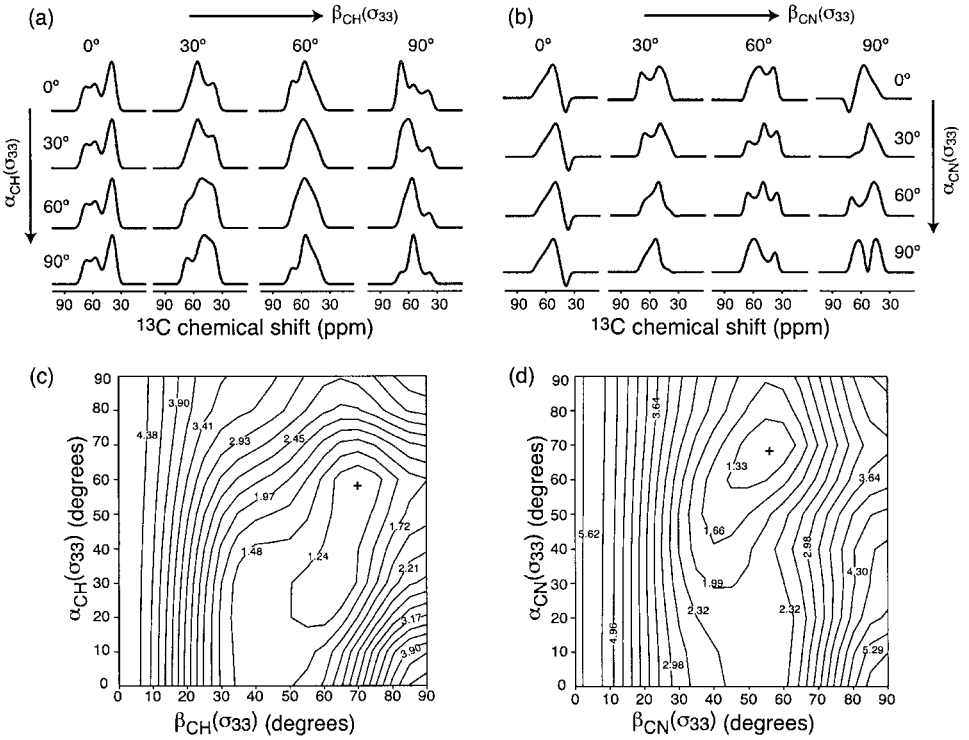

Figure 5. Simulated Cα–Hα (a) and Cα–N (b) modulated Cα CSA spectra of Ala as a function of the orientation of the Cα–Hα(N) bond. The best fit (cross) is found as the minimum in the 2D RMSD contour plot for the Cα–Hα modulation experiment (c) and the Cα–N modulation experiment (d). These give $\beta_{CH}(\sigma_{33}) = 70^o \pm 5^o$, $\alpha_{CH}(\sigma_{33}) = 58° \pm 10°$, $\beta_{CN}(\sigma_{33}) = 56° \pm 5°$, and $\alpha_{CN}(\sigma_{33}) = 68° \pm 10°$.

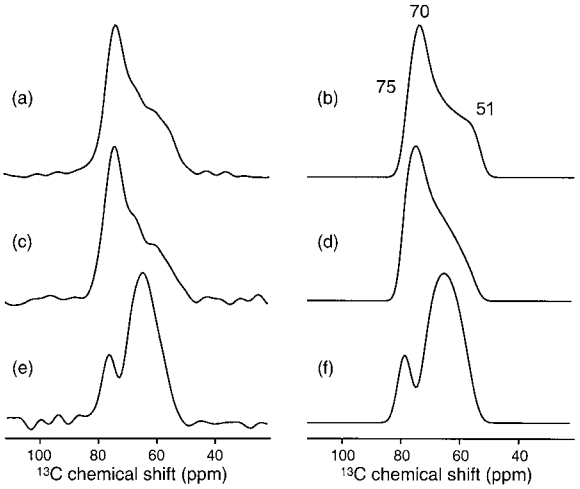

Figure 6. Recoupled CSA spectra of Val Cα in GG*V, extracted from the indirect dimension of various 2D spectra. (a) CSA powder pattern without dipolar modulation. NS per t_1 slice = 192. (b) Best-fit spectrum of (a). (c) Cα–Hα modulated CSA spectrum, acquired with a CP contact time of 20 μs. NS per t_1 slice = 192. (d) Best-fit spectrum for (c), using $\beta_{CH}(\sigma_{33}) = 65°$ and $\alpha_{CH}(\sigma_{33}) = 20°$. (e) Cα–N modulated CSA spectrum, acquired with a C–N dephasing time of 4 ms. NS per t_1 slice = 512. (f) Best-fit spectrum for (e), using $\beta_{CN}(\sigma_{33}) = 82°$ and $\alpha_{CN}(\sigma_{33}) = 62°$. All 2D spectra were obtained with a maximum evolution time of 11.2 ms.

To resolve this near degeneracy between the σ_{11} and σ_{22} axis orientations, we carried out a complementary Cα–Hα modulation experiment that relies on C–H dipolar dephasing rather than C–H build-up, which is inherent to the short CP experiment, to modulate the Cα powder pattern. The dephasing experiment inserts a short period (about 30 μs) without ^{1}H decoupling into the SUPER experiment, while the initial CP contact time is allowed to be long to create full ^{13}C magnetization. The Cα magnetization dephases under the Cα–Hα dipolar coupling for the undecoupled period before CSA evolution. This dephasing experiment allows the observation of low or negative intensities at the frequency position closest to parallel to the Cα–Hα bond. Thus it offers an alternative way of distinguishing the δ_{11} and δ_{22} positions of the Cα powder pattern. Figure 8(a) shows the experimental Val Cα spectrum dephased by 30 μs of Cα–Hα coupling, where the sample was spun at 1.8 kHz to satisfy the quasi-static condition. For comparison, the simulated spectra for the two possible orientations of the σ_{11} and σ_{22} axes are shown in Figure 8(b–c). The comparison indicates that the σ_{11} axis is closer to be-

ing parallel to the Cα–Hα bond than perpendicular to it, with $\beta_{CH}(\sigma_{11}) = 32°$. Spectrum simulated using the quantum chemical calculated angle of $\beta_{CH}(\sigma_{11}) = 97°$ is also shown (Figure 8d), and is found to be inconsistent with the experimental spectra in the relative intensities of the δ_{11} and δ_{22} edges. Similarly, we analyzed the Cα–N modulated spectrum with the two possibilities of the σ_{11} and σ_{22} axis orientations. The experimental spectrum (Figure 8(e)) shows positive intensities at ∼77 ppm, which is consistent with $\beta_{CN}(\sigma_{11}) = 62°$ but inconsistent with the complementary angle of 28°, nor with the quantum chemical prediction of $\beta_{CN}(\sigma_{11}) = 20°$.

Solutions for the Ala and Val Cα tensor orientations

In principle, the dipolar-modulated experiments give a number of degenerate orientations for the chemical shift tensor. For example, the σ_{33} axis can have two possible orientations based on a unique $\beta_{CH}(\sigma_{33})$ and a unique $\beta_{CN}(\sigma_{33})$. These two orientations correspond to the intersections of the two cones around the Cα–Hα bond and the Cα–N bond with cone semi-angles of $\beta_{CH}(\sigma_{33})$ and $\beta_{CN}(\sigma_{33})$, respectively. The fact that each polar angle has a two-fold degeneracy within a 180° range increases the number of possible principal axis orientations. As a result, a total of 8 orientations are possible for each principal axis, when the experimentally determined angles for each axis are examined separately. However, when the orientations of the three principal axes are considered together, most solutions are ruled out by the molecular geometry, and by the requirement that the three principal axes form a right-handed Cartesian coordinate system.

The orientations of the Ala and Val Cα chemical shift tensors in the molecular frame are shown in Figure 9. For G*AL, two solutions that satisfy both the molecular geometry and the experimental results were found. The solution closer to the quantum chemical calculations is shown in Figure 9(a). The angles between σ_{11}, σ_{22}, σ_{33} and the Cα–Hα bond are 116°, 146° and 70°, respectively. On the other hand, the Cα–N bond is 108°, 40° and 56° from the σ_{11}, σ_{22}, and σ_{33} axis, respectively. For GG*V, the σ_{33} axis forms an angle of 98° from the Cα–N bond and 115° from the Cα–Hα bond (Figure 9(b)). This is unambiguous from the experiments, since the σ_{33} axis is the main principal axis of the tensor. The σ_{11} axis is 155° from the Cα–Hα bond and 63° from the Cα–N bond. These angles, which are constrained by the molecular geometry and the Cartesian coordinate system, deviate from the best-fit values by 7°–17°, reflecting the uncertainties in the angle determination.

Comparison with ab initio calculations

The experimentally determined magnitude and orientation of the Ala and Val CSA tensors are listed in Table 1, along with the calculated Cα shielding tensors for the same torsion angles (Sun et al., 2002). The torsion angles were taken from the crystal structure that is either available in the literature (Lalitha et al., 1984) or directly measured on the NMR sample.

Ab initio calculations predicted an Ala Cα CSA span of about 30 ppm for both helix and sheet conformations with relatively small differences (Havlin et al., 1997). We measured a span of 35 ppm in GAL. The experimental asymmetry parameter is 0.89, compared to 0.91 from calculation. The experimental angles between the σ_{11}, σ_{22}, and σ_{33} axis and the Cα–Hα bond are 116°, 146° and 70°, respectively, while the corresponding calculated angles are 108°, 160° and 82°. Thus, the calculated angles differ from experiments only by 8°–14°. The orientations of the three principal axes relative to the Cα–N bond are 108° for σ_{11}, 40° for σ_{22} and 56° for σ_{33}. The calculated values are 114°, 53° and 47°, again in good agreement (6°–13° deviations) with the experimental results. The Ala tensor results confirm the prediction that the σ_{11} principal axis is roughly perpendicular to the Cα–Hα bond in the helical conformation. This contrasts with the σ_{11} orientation of β-sheet Val, where the σ_{11} axis is 22° from the Cα–Hα bond (Yao and Hong, 2002). The experimental Val Cα CSA span in GGV is 24 ppm, which is only 1.4 ppm apart from the predicted value of 22.6 ppm. This is more than 20 ppm smaller than the span of the β-sheet Val in NAV (Yao and Hong, 2002), which is 46.5 ppm. This large distinction between helical and sheet CSA span is well predicted by theory (Oldfield, 1995). The asymmetry parameter of the helical Val is 0.33 from experiment and 0.23 from calculation, again in good accord with each other. The experimental angle between σ_{33} and the Cα–Hα bond is 115°, which is only 8° different from the calculated angle of 107°. The experimental σ_{33} to Cα–N angle is 98°, compared to a calculated value of 99°. Thus, the calculated orientation of the main principal axis of the Val tensor agrees with our experimental measurement closely.

As discussed above, the near-uniaxiality of the Val tensor, manifested as only a 5 ppm difference between the δ_{11} and δ_{22} principal values, renders the

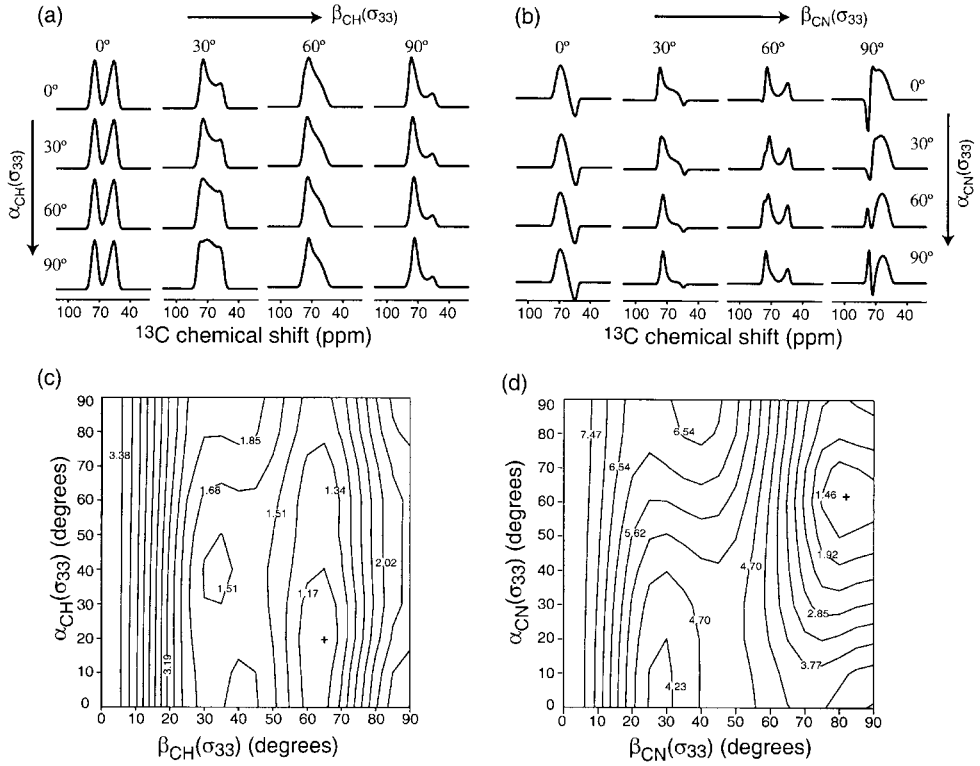

Figure 7. Simulated Cα–Hα modulated (a) and Cα–N modulated (b) CSA spectra of GG*V as a function of the orientation of the Cα–Hα(N) bond. The best fit (cross) is found as the minimum in a 2D RMSD contour plot for the Cα–Hα modulation experiment (c) and the Cα–N modulation experiment (d). These give $\beta_{CH}(\sigma_{33}) = 65° \pm 5°$, $\alpha_{CH}(\sigma_{33}) = 20° \pm 30°$, $\beta_{CN}(\sigma_{33}) = 82° \pm 5°$, and $\alpha_{CN}(\sigma_{33}) = 62° \pm 30°$.

orientations of the σ_{11} and σ_{22} axes more difficult to distinguish. However, both the CP-based Cα–Hα modulation experiment and the Cα–Hα dipolar dephasing experiment support the conclusion that the σ_{11} axis in GGV is more closely aligned with the Cα–Hα bond than the σ_{22} axis is. This differs from the quantum chemical calculation. We hypothesize that for such nearly uniaxial tensors, factors other than local torsion angles, such as intermolecular packing and hydrogen bonding with water, may significantly influence the orientation of the Cα tensor. Such factors would exist in a realistic sample but is not taken into account in *ab initio* calculations. The C-terminus inductive effect may also influence the Cα tensor orientation. However, according to the crystal structure of GGV, both oxygen atoms of the valine carboxyl group are involved in hydrogen bonding. This means the negative charge on the C-terminus is shared by the hydrogen-bonded protons, thus the inductive effects should be very weak.

Comparison between the experimental chemical shifts and calculated chemical shielding for the three peptides – GAL, GGV and NAV – is best made using an icosahedral representation (Alderman et al., 1993). This formalism is attractive since it allows both the magnitude and orientation of the tensors to be compared as the six principle values along the six apolar directions of an icosahedron. These directions are defined by connecting the 12 vertices of an icosahedron with lines through its center. Both the experimental shift and the theoretical shielding tensors are rotated from their respective Cartesian PAS frames to a common molecular frame and then to an icosahedral frame. The transformation from the Cartesian system to the icosahedral system involves straightforward analytical expressions converting the nine Cartesian matrix elements of the tensor to the six diagonal elements in the icosahedron system (Alderman et al., 1993). Once the experimental and calculated tensors are expressed in the icosahedral representation, the theoretical chemical shielding values can be plotted against the corresponding experimental chemical shift values.

Table 1. Summary of Val and Ala Cα CSA tensors from experiments and *ab initio* calculations (Sun et al., 2002)

	GG*V		G*AL		
	Experiment	Calculation[a]	Experiment		Calculation[a]
ϕ	−81.5°	−81.5°	−65.7°		−65.7°
ψ	−50.7°	−50.7°	−40°		−40°
χ	180°	180°			
δ_{11} (ppm)	75		70		
σ_{11} (ppm)		128.9		126.7[b]	
δ_{22} (ppm)	70		51		
σ_{22} (ppm)		132.1		141.3[b]	
δ_{33} (ppm)	51		35		
σ_{22} (ppm)		151.5		158.2[b]	
δ_{iso} (ppm)	65.3		52.0		
σ_{iso} (ppm)		137.5		142.1[b]	
Ω (ppm)	24	22.6	35		31.5
η	0.33	0.23	0.89		0.91
σ_{11}-CH angle (°)	155[d]	97	116[d]	116[d]	108
σ_{22}-CH angle (°)	89[d]	161	146[d]	146[d]	160
σ_{33}-CH angle (°)	115[c,d]	107	70[d]	110[c,d]	82
σ_{11}-CN angle (°)	63[d]	19	108[d]	108[d]	114
σ_{22}-CN angle (°)	28[d]	74	40[d]	40[d]	53
σ_{33}-CN angle (°)	98[c,d]	99	56[c,d]	124[c,d]	47

[a]Obtained from Sun et al. (2002).
[b]Obtained from the chemical shielding calculator at http://waugh.cchem.berkeley.edu/~bob/cs.html
[c]Angles directly obtained from simulations of the experimental spectra. For GGV, these are the most reliable angles.
[d]The error bars for the experimentally determined orientation angles are ± 5°, except for the orientations of the σ_{11} and σ_{22} axes of GG*V, which have an uncertainty of ±10°.

Figure 10 displays the comparison between the experimental shift and the calculated shielding for GAL, GGV, and NAV, using this icosahedral representation. A clear linear correlation is observed between experiment and calculation. Linear regression analysis of the data yielded slopes (m) of −0.77 to −0.95 and correlation coefficients (R) from 0.91 to 0.98 for the three peptides. These indicate good agreement between the experiments and calculations. The fact that the slopes deviate from −1 suggests small systematic errors in the calculated chemical shielding tensors that may result from factors other than backbone torsion angles. Among the three peptides, NAV and GAL have less scatter than GGV, as indicated by their higher R values as well as the smaller relative RMSD values, which are defined as the ratio of RMSD to the anisotropic span Ω. The better fit for GAL and NAV is understandable, since GGV is the only compound with significantly different σ_{11} and σ_{22} orientations between the experimental and calculated tensors. However, the comparison in the icosahedral representation shows clearly that the impact of such an orientation deviation is relatively minor, due to the near uniaxiality of the σ_{11} and σ_{22} elements.

Figure 10(d) combines the icosahedral representation for all three peptides, where both the isotropic shift and the isotropic shielding are set to 0 ppm. Interestingly, this procedure resulted in overall better agreement between theory and experiments, as manifested by a slope of 0.88, a correlation coefficient of 0.94, and an RMSD of 1.9 ppm.

Comparison with solution NMR

Since $\Delta\sigma^* = \sigma_{orth} - \sigma_{par}$ have been shown to correlate strongly with protein secondary structure, we converted the CSA tensors determined here to $\Delta\sigma^*$. The conversion was made according to Tjandra and

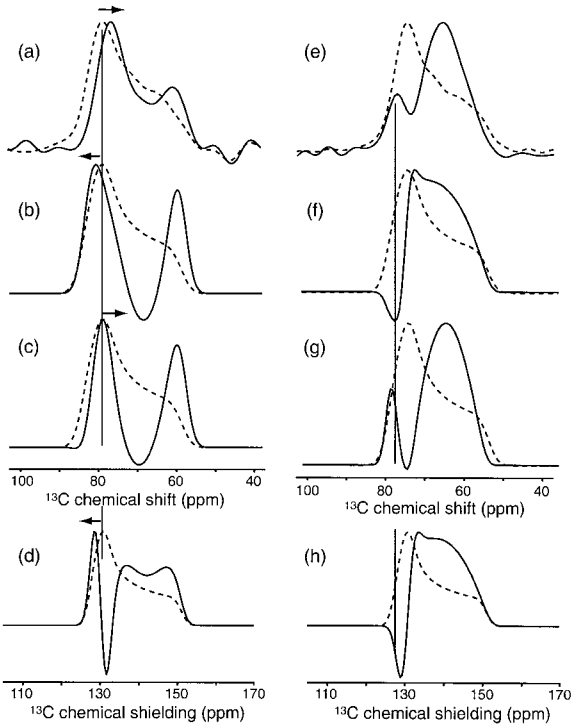

Figure 8. Cα–Hα dephased (left column) and Cα–N dephased (right column) Val spectra of GGV. The full CSA powder pattern without modulation (dashed lines) is superimposed with each dephased spectrum (solid). (a) Experimental Cα–Hα dephased spectrum, after a dephasing time of 30 μs. Simulated spectra are for (b) $\beta_{CH}(\sigma_{11}) = 72°$, (c) $\beta_{CH}(\sigma_{11}) = 32°$, and (d) $\beta_{CH}(\sigma_{11}) = 96.8°$. (e) Experimental Cα–N dephased spectrum with 4 ms dephasing. Simulated Cα-N dephased spectra for (f) $\beta_{CN}(\sigma_{11}) = 28°$, (g) $\beta_{CN}(\sigma_{11}) = 62°$, and (h) $\beta_{CN}(\sigma_{11}) = 18.8°$.

Table 2. $\Delta\sigma^*$ values of three model peptides, obtained from the experimentally determined chemical shift principal values and principal axes orientations

Peptides	ϕ (°)	ψ (°)	$\Delta\sigma^*$ (ppm)
G*AL	−65.7	−40	1.9
GG*V	−81.5	−50.7	8.3
NA*V	−136.5	178.2	28.9

Bax (1997):

$$\sigma_{par} = \sigma_{11}cos^2(\beta_{CH}(\sigma_{11})) + \sigma_{22}cos^2(\beta_{CH}(\sigma_{22})) + \sigma_{33}cos^2(\beta_{CH}(\sigma_{33})), \quad (3)$$

$$\Delta\sigma^* = \sigma_{orth} - \sigma_{par} = 1.5 * (\sigma_{iso} - \sigma_{par}). \quad (4)$$

To obtain the shielding values σ_{ii} from the chemical shifts δ_{ii}, we used the absolute shielding of liquid TMS at room temperature (Jameson and Jameson, 1987)

$$\delta_{ii} = 184.1 - \sigma_{ii} \quad (5)$$

Table 2 lists the $\Delta\sigma^*$ values for helical Ala and Val and for the β-sheet Val measured in NAV. The experimental $\Delta\sigma^*$ is 1.9 ppm for helical Ala and 8.3 ppm for helical Val. However, a much larger $\Delta\sigma^*$ of 28.9 ppm was obtained for the β-sheet Val in NAV. A similar calculation of $\Delta\sigma^*$ for several solid peptides was made recently, in which the experimental CSA principal values obtained from sideband intensities were combined with the calculated tensor orientations (Havlin et al., 2001). That study found $\Delta\sigma^*$ values of less than 10 ppm for the helical residues but about 30 ppm for the sheet conformation, consistent with our current results.

Conclusions

In summary, we have determined both the orientation and the magnitude of the Cα chemical shift tensors of Ala and Val in the helical conformation using dipolar modulated CSA recoupling experiments. We found that in helical Ala, the σ_{11} axis is 116° ± 5° from the Cα–Hα bond and 108° ± 5° from the Cα–N bond. Thus, the helical Ala σ_{11} axis is roughly perpendicular to the Cα–Hα bond, in contrast to the β-sheet Val in NAV, whose σ_{11} axis is nearly parallel (22°) to the Cα-Hα bond. The anisotropic span of the helical Ala is 36 ppm. In helical Val, the Cα CSA span is 25 ppm, almost a factor of two smaller than in β-sheet Val. The σ_{33} axis is 115° ± 5° from the Cα–Hα bond and 98° ± 5° from the Cα–N bond. The tensor is nearly uniaxial, with the δ_{11} and δ_{22} principal values differing by only 5 ppm. Detailed C–H dephasing experiment showed that the σ_{11} axis is 155° ± 10° from the Cα–Hα bond and 63° ± 10° from the Cα–N bond. The experimentally determined chemical shift tensors are compared with quantum chemical calculations using an icosahedral representation. This comparison yielded linear least-square fits with correlation coefficients larger than 0.9, indicating good agreement between theory and experiment. Converting the experimental chemical shift principal values and principal axis orientations to $\Delta\sigma^*$, we found small $\Delta\sigma^*$ values for the helical Val (8.3 ppm) and Ala (1.9 ppm), but a large $\Delta\sigma^*$ value for the β-sheet Val (28.9 ppm). Thus, $\Delta\sigma^*$ is an excellent indicator for the backbone conformation of peptides and proteins. Even for a chemical

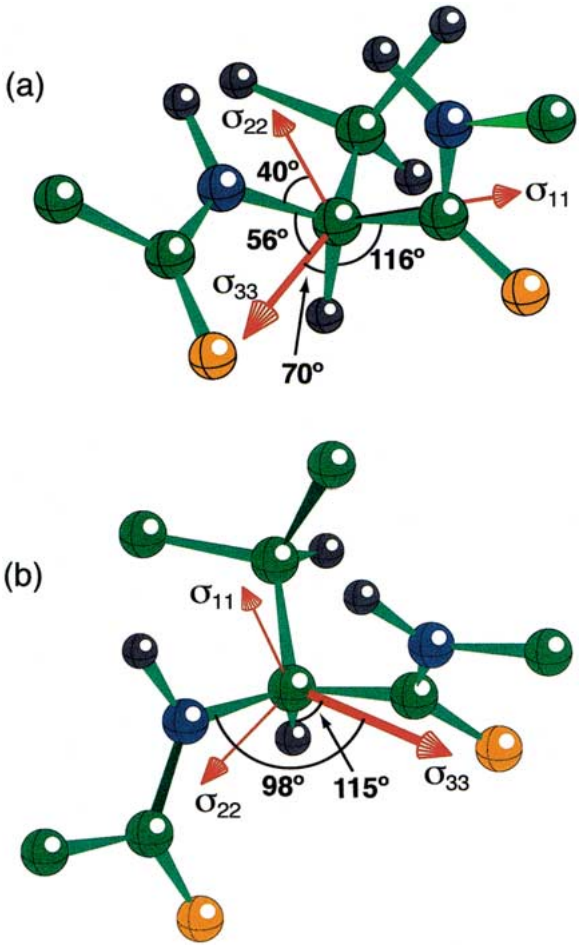

Figure 9. Orientation of the Cα chemical shift tensor of helical Ala (a) and Val (b).

shift tensor with a large span, such as that of Ala in GAL, $\Delta\sigma^*$ is very small in the helix conformation due to the tensor orientation.

The ability to determine the Cα tensor orientations in peptides with site resolution opens up new possibilities for distinguishing protein secondary structures using solid-state NMR. Spectral editing experiments (Hong, 2000) incorporating both the CSA magnitude and orientation can be conceived. These can be used to better identify backbone conformations and to refine the structure measured via other parameters such as torsion angles (Weliky and Tycko, 1996; Costa et al., 1997; Feng et al., 1997; Hong et al., 1997; Bower et al., 1999).

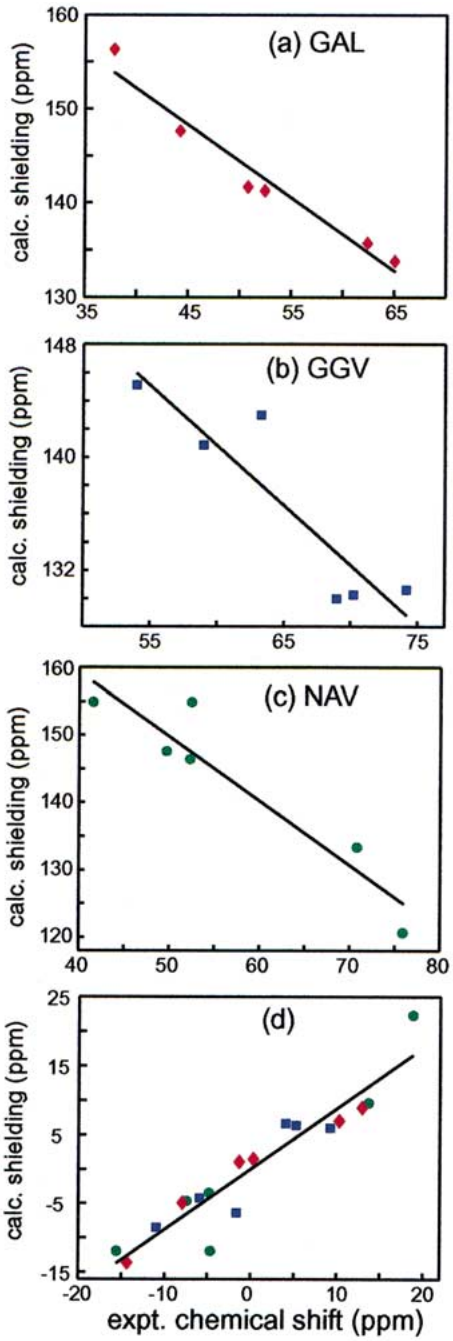

Figure 10. Comparison between experimental chemical shifts and calculated chemical shielding in the icosahedral representation. (a) G*AL. Linear least square fit parameters: slope m = −0.77, intercept y_0 = 183.2 ppm, R = 0.98, and RMSD = 1.6 ppm (4.4%). (b) GG*V. m = −0.85, y_0 = 191.7 ppm, R = 0.91, and RMSD = 2.7 ppm (10.8%). (c) NA*V. m = −0.95, y_0 = 197.5 ppm, R = 0.94, and RMSD = 4.1 ppm (8.8%). (d) Combined data from all three peptides. The isotropic shift and isotropic shielding are set to zero according to $\delta' = \delta - \delta_{iso}$ and $\sigma' = \sigma_{iso} - \sigma$. GAL (diamond), GGV (square), and NAV (circle). m = 0.88, y_0 = 0 ppm, R = 0.94, and RMSD = 1.9 ppm.

Acknowledgements

The authors thank Laura Dutca for help in peptide synthesis and Professor R. Wittebort for useful discussions about peptide purification. Stimulating discussions with Professor Oldfield are gratefully acknowledged. This work is partially supported by a Research Innovation award from the Research Corporation and a National Science Foundation CAREER award to M.H. (MCB-0093398).

References

Alderman, D.W., Sherwood, M.H. and Grant, D.M. (1993) *J. Magn. Reson.*, **A101**, 188–197.

Bennett, A.E., Rienstra, C.M., Auger, M., Lakshmi, K.V. and Griffin, R.G. (1995) *J. Chem. Phys.*, **103**, 6951–6958.

Bower, P.V., Oyler, N., Mehta, M.A., Long, J.R., Stayton, P.S. and Drobny, G.P. (1999) *J. Am. Chem. Soc.*, **121**, 8373–8375.

Carroll, P.J., Stewart, P.L. and Opella, S.J. (1990) *Acta Cryst.*, **C46**, 243–246.

Chaturvedi, S., Go, K. and Parthasarathy, R. (1991) *Biopolymers*, **31**, 397–407.

Costa, P.R., Gross, J.D., Hong, M. and Griffin, R.G. (1997) *Chem. Phys. Lett.*, **280**, 95–103.

Dixon, W.T. (1982) *J. Chem. Phys.*, **77**, 1800–1809.

Duncan, T.M. (1997) *Chemical Shift Tensors*, 2nd edn, Farragut Press, Madison, Wisconsin.

Feng, X., Eden, M., Brinkmann, A., Luthman, H., Eriksson, L., Graslund, A., Antzutkin, O.N. and Levitt, M.H. (1997) *J. Am. Chem. Soc.*, **119**, 12006–12007.

Harris, R.K. and Oliveri, A.C. (1992) *Prog. NMR Spectrosc.*, **24**, 435–456.

Hartzell, C.J., Pratum, T.K. and Drobny, G. (1987) *J. Chem. Phys.*, **87**, 4324–4331.

Hartzell, C.J., Whitfeld, M., Oas, T.G. and Drobny, G.P. (1987) *J. Am. Chem. Soc.*, **109**, 5966–5969.

Havlin, R.H., Laws, D.D., Bitter, H.L., Sanders, L.K., Sun, H., Grimley, J.S., Wemmer, D.E., Pines, A. and Oldfield, E. (2001) *J. Am. Chem. Soc.*, **123**, 10362–10369.

Havlin, R.H., Le, H., Laws, D.D., deDios, A.C. and Oldfield, E. (1997) *J. Am. Chem. Soc.*, **119**, 11951–11958.

Hong, M. (2000) *J. Am. Chem. Soc.*, **122**, 3762–3770.

Hong, M., Gross, J.D. and Griffin, R.G. (1997) *J. Phys. Chem.*, **B101**, 5869–5874.

Jameson, A.K. and Jameson, C.J. (1987) *Chem. Phys. Lett.*, **134**, 461–466.

Jameson, C.J. (1998) *Solid State NMR*, **11**, 265–268.

Lalitha, V., Subramanian, E. and Bordner, J. (1984) *Int. J. Pept. Protein Res.*, **24**, 437–441.

Liu, S.F., Mao, J.D. and Schmidt-Rohr, K. (2002) *J. Magn. Reson.*, **155**, 15–28.

Oldfield, E. (1995) *J. Biomol. NMR*, **5**, 217–225.

Schmidt-Rohr, K. and Spiess, H.W. (1994) *Multidimensional Solid-State NMR and Polymers*, Academic Press, San Diego, California.

Sitkoff, D. and Case, D.A. (1998) *Prog. NMR Spectrosc.*, **32**, 165–190.

Spera, S. and Bax, A. (1991) *J. Am. Chem. Soc.*, **113**, 5490–5492.

Sun, H., Sanders, L.K. and Oldfield, E. (2002) *J. Am. Chem. Soc.*, submitted.

Tjandra, N. and Bax, A. (1997) *J. Am. Chem. Soc.*, **119**, 9576–9577.

Tycko, R., Dabbagh, G. and Mirau, P. (1989) *J. Magn. Reson.*, **85**, 265–274.

Walling, A.E., Pargas, R.E. and deDios, A.C. (1997) *J. Phys. Chem.*, **A101**, 7299–7303.

Weliky, D. and Tycko, R. (1996) *J. Am. Chem. Soc.*, **118**, 8487–8488.

Wishart, D.S., Sykes, B.D. and Richards, F.M. (1991) *J. Mol. Biol.*, **222**, 311–333.

Yao, X.L. and Hong, M. (2002) *J. Am. Chem. Soc.*, **124**, 2730–2738.